Atmos. Chem. Phys. Discuss., 10, 17369–17405, 2010
www.atmos-chem-phys-discuss.net/10/17369/2010/
doi:10.5194/acpd-10-17369-2010

Atmospheric Chemistry and Physics Discussions

Physico-chemical characterization of secondary organic aerosol derived from catechol and guaiacol as a model substance for atmospheric humic-like substances

J. Ofner[1], H.-U. Krüger[1], H. Grothe[2], P. Schmitt-Kopplin[3,5], K. Whitmore[4], and C. Zetzsch[1]

[1]Atmospheric Chemistry Research Laboratory, University of Bayreuth, Germany
[2]Institute of Materials Chemistry, Vienna University of Technology, Austria
[3]Institute of Ecological Chemistry, Helmholtz Zentrum Munich, Germany
[4]University Service Centre for Transmission Electron Microscopy, Vienna University of Technology, Austria

[5] Department for Chemical-Technical Analysis, Research Center Weihenstephan for Brewing and Food Quality, Technical University Munich, Freising-Weihenstephan, Germany

Received: 28 June 2010 – Accepted: 29 June 2010 – Published: 20 July 2010

Correspondence to: H. Grothe (grothe@tuwien.ac.at)

Published by Copernicus Publications on behalf of the European Geosciences Union.

ACPD
10, 17369–17405, 2010

Abstract

Secondary organic aerosol was produced from the aromatic precursors catechol and guaiacol by reaction with ozone in the presence and absence of simulated sunlight and humidity and investigated for its properties as a proxy for humic-like substances (HULIS). Beside a small particle size, a relatively low molecular weight and typical optical features in the UV/VIS spectral range, HULIS contain a typical aromatic and/or olefinic chemical structure and highly oxidized functional groups within a high chemical diversity. Various methods were used to characterize the secondary organic aerosols obtained: Fourier transform infrared spectroscopy (FTIR) demonstrated the formation of different carbonyl containing functional groups as well as structural and functional differences between aerosols formed at different environmental conditions. UV/VIS spectroscopy of filter samples showed that the particulate matter absorbs far into the visible range up to more than 500 nm. Ultrahigh resolved mass spectroscopy (ICR-FT/MS) determined O/C-ratios between 0.3 and 1 and main molecular weights between 200 and 500 Da. Temperature-programmed-pyrolysis mass spectroscopy identified carboxylic acids and lactones as major functional groups. Particle sizing using CNC-DMPS demonstrated the formation of small particles during a secondary organic aerosol formation process. Particle imaging using field-emission-gun scanning electron microscopy (FEG-SEM) showed spherical particles, forming clusters and chains. Hence, secondary organic aerosols from catechol and guaiacol are appropriate model substances for studies of the processing of aromatic secondary organic aerosols and atmospheric HULIS on the laboratory scale.

1 Introduction

Atmospheric aerosol particles strongly influence the global atmosphere, and their contribution to climate change is manyfold (Forster et al., 2007). Especially secondary organic aerosols (SOA) play a major role in the impact of atmospheric chemistry on

ACPD
10, 17369–17405, 2010

climate. Mass fluxes of 30–270 Tg year^{-1} are estimated to be emitted per year by tropospheric oxidation of biogenic and anthropogenic volatile organic compounds (Andreae and Crutzen, 1997). However, formation pathways of SOA are still incompletely clarified, and details of the initiating reactions and therefore, the chemical transformation of the precursors by atmospheric oxidizing trace gases are hardly known.

The best-known process is the formation of SOA from α-pinene (e.g., Jonsson et al., 2007). Aerosol chamber studies have been applied to investigate particle formation and processing (Iinuma et al., 2004). The transformation pathways of this model substance have been well characterized by many authors, and various gaseous intermediates, such as pinonaldehyde, pinene oxide, norpinaldehyde and 4-oxopinonaldehyde have been summarized in a recent overview (Yu et al., 2008), although the reported yields of pinonaldehyde span a range from 0.3 to 53 wt.% in the O_3-reaction and 6–87 wt.% in the OH-reaction. Even the influence of water on aerosol formation of α-pinene has been studied (Jonsson et al., 2008).

Recently, atmospheric HUmic LIke Substances (HULIS) have attracted more interest than pure aliphatic organic aerosols. This special class of organic aerosols was termed HULIS because of their apparent similarity to humic substances found in environmental soil and water samples. This naming was based on their macromolecular structure, causing a brownish (from light yellow to black) colour, their solubility in water (WSOC) and other properties, derived using methods to describe overall parameters of organic macromolecules. But there is still an intense discussion about their humic character, as Graber and Rudich (2006) have summarized. For SOA formation from other precursors, especially from simple aromatic molecules which might be typical HULIS precursors, the current knowledge is still rather poor. The physical chemical properties of atmospheric HULIS strongly differ from humic substances of any other environmental domain (soil, waters). Major portions of atmospheric HULIS originate from volatile organic compounds, forming SOA by abiotic oxidizing reactions and do not originate from primary soil emissions. Thus performing aerosol smog-chamber studies with HULIS, representative HULI-SOA precursors are needed as model substances

ACPD
10, 17369–17405, 2010

in order to generate SOA with HULIS qualities in-situ in an aerosol-smog-chamber (Cowen and Al-Abadleh, 2009). An appropriate candidate is catechol, which is also reported as a strong emission from open biomass burning (Hays et al., 2005) and fireplace combustion (Fine et al., 2002) leading to so-called biomass-burning organic aerosols (BBOA).

Aerosol formation from catechol has been studied very recently (Coeur-Tourneur et al., 2009), obtaining large mass yields ranging from 17 to 86 wt.% in a smog chamber in the presence of ozone with only minor influence of self-produced OH, which is known from scavenger experiments to enhance the consumption of catechol by 30% (Tomas et al., 2003). The rate constant for the reaction of catechol with O_3 has been determined to be 9.6×10^{-18} cm^3 s^{-1} at 298 K, and the vicinal OH groups have been suggested as a potential cause of the high ozone reactivity of catechol (Tomas et al., 2003). The gas-phase reaction of dihydroxybenzenes with OH radicals has been studied in detail (Olariu et al., 2000). Furthermore, infrared spectroscopy of the oxidation of catechol has been performed in aqueous phase (Khovratovich et al., 1998). Nieto-Gligorovski et al. (2008, 2010) studied oxidation reactions of 4-carboxybenzophenone/catechol films using UV/VIS and FTIR spectroscopy. They report a photosensitized oxidation of the phenolic precursor by ozone in the presence of simulated sunlight to form products with properties similar to HULIS. Processing of catechol aerosol has been studied recently (Broeske et al., 2003).

In the recent past several field studies of SOA have been performed using aerosol mass spectroscopy as a powerful tool identifying a myriad of compounds. However, the analyses of these data show that complete single-molecule identification is a rather impossible task due to strong fluctuations of the chemical composition of the aerosol and due to the occurrence of isobaric substances. At current, half of the particulate organic matter (POM) cannot be characterized as individual compounds. POM contains numerous types of organic molecules including hydrocarbons, alcohols, aldehydes, and carboxylic acids (Limbeck et al., 2005; Kundu et al., 2010). Therefore, the more leading approach is focusing on the reactive functional groups and fading out the aliphatic

ACPD
10, 17369–17405, 2010

or aromatic rest. A new concept of laboratory and field measurements is needed, which aims at the understanding of the dynamic properties of SOA. Organic matter is semi-volatile and thus readily exchanges between gas and aerosol phase. Oxidation and oligomerization leads to larger molecules and thus changes the physical-chemical parameter of the aerosol completely.

Aerosol and smog chambers are at the intersection between field analytics and laboratory characterizations. Thus they should also be well-suited for the controlled preparation and supply of model substances. However, traditional SOA models based on smog chamber experiments do not fit the actual requirements and do not include the aging properties, which have been observed in field experiments and are particularly important when discussing HULIS properties. Hence, in the Bayreuth aerosol-smog-chamber a new approach has been developed, where a catechol-aerosol model system has been chosen and has been analysed in time dependence under defined photochemical conditions. Especially different relative humidities have been simulated playing an important role in aerosol formation and/or processing (Vesna et al., 2009), and the hygroscopicity of the particle relates to the degree of oxidation. Beside aerosol size distributions, spectral characterisation of those aerosol particles is of utmost interest. A variety of methods is available to study atmospheric surfaces and their interaction with atmospheric trace gases (Zellner et al., 2009). Particularly, surface functional groups are reaction sites for heterogeneous aerosol chemistry (Lary et al., 1999). For studying the formation and processing of those functional groups Fourier transform infrared spectroscopy is most suitable (Najera et al., 2009). Time resolved FTIR spectroscopy of the formation of organic aerosol particles was applied by Sax et al. (2005). Coury and Dillner (2008) used ATR-FTIR spectroscopy to quantify organic functional groups in ambient aerosols. Secondary organic aerosols are characterized by their particle size distributions. Furthermore, light-absorption of organic materials plays an important role for the radiative forcing (Shapiro et al., 2009). To complete and confirm spectroscopic results ultrahigh resolution mass spectroscopy (ICR-FT/MS) and imaging by electron microscopy are used in the present study.

ACPD
10, 17369–17405, 2010

2 Methods

HULI-SOA is a rather complex mixture of different organic macromolecules with various oxygenated functional groups. A single-molecule analysis has turned out to be rather useless. Therefore, in the focus of our analytic strategy are techniques which determine the functional groups, the O/C ratio, and the particle's morphology. Changes during the photo-oxidation shall be revealed and a well-characterized model substance will be defined.

2.1 Aerosol smog chamber

All secondary organic aerosols were produced in a cylindrical 700-L aerosol smog chamber made of Duran glass. Fluorinated ethylene propylene film (FEP) covers both ends of the cylinder and serves as window for a solar simulator, equipped with a medium-pressure metal vapour lamp (Osram HMI, 4000 W). A water cooled glass plate cuts off the UV-C range of the lamp spectrum. The one centimetre thick water film reduces the entry of infrared radiation from the HMI lamp into the smog chamber. The smog chamber is flushed with particle-free air produced using a zero air generator (CMC ZA 50 K). The ozone concentration at the beginning of the experiments was measured using a chemiluminescence ozone analyser (UPK 8002).

2.2 Aerosol size distribution

Aerosol particle concentrations were recorded using a condensation nucleus counter (CNC, TSI 3020). An electrostatic classifier (TSI 3071) with a neutralizer (^{85}Kr), coupled to the CNC, was used to determine the aerosol size distribution.

2.3 Electron microscopy

Images of the formed aerosol particles were taken using a FEI Quanta 200 Field Emission Gun Scanning Electron Microscope (FEG-SEM). Therefore particles were col-

ACPD
10, 17369–17405, 2010

lected using Isopore^{TM} membrane filters (Millipore) made of polycarbonate with a pore size of about 50 nm. The aerosol particles were protected against electric charging by sputtering 3–4 nm of Au/Pd onto their surface. The FEG-SEM was operating at 6×10^{-6} mbar using a cathode voltage of 5 kV to avoid high penetration depth and just image the surface.

2.4 Long-path FTIR spectroscopy

For long-path absorption, the chamber is equipped with a 40 m White-cell coupled to a FTIR spectrometer (Bruker IFS 113v). The instrument is evacuated down to 60 mbar to diminish disturbance of the spectra by atmospheric compounds. Long-path FTIR spectra were recorded at a spectral resolution of 2 cm^{-1} from 4000 to 580 cm^{-1} using a MCT detector and accumulating 256 single interferograms each. Post processing and atmospheric compensation of the infrared spectra was performed using the Bruker Opus software package (version 5.0).

2.5 Attenuated Total Reflectance (ATR) infrared spectroscopy

The aerosol particles were deposited onto the KRS-5 ATR crystal (52×20×2 mm, trapezoidal) for ATR-FTIR spectroscopy between 4000 and 400 cm^{-1} using a self developed electrostatic precipitator (ESP). For sampling of aerosol particles onto a KRS-5 crystal, which was not possible with the former prototype described by Ofner et al. (2009), a two-stage precipitator was developed and is illustrated in Fig. 1. The precipitator is based on the concepts of Fierz et al. (2007) and Mainelis et al. (2002). This ESP has a separate charging and deposition zones. The ESP is operated at high voltages of about 10.5 kV. After entering the ESP the aerosol particles are charged by a corona discharge and accelerated towards a bevelled deflector at 3.5 kV. The high voltage between the deflector and the ground plate of 7 kV turns the aerosol flight path towards the ATR crystal. Using an electrometer between the copper plate and the ground connection allows us to observe the electric current flowing off the ATR crystal (Fig. 1).

ACPD
10, 17369–17405, 2010

For developing this ESP, the electric field between the needle, the deflector and the ATR crystal was calculated using the software Student's QuickField 5.5 (Tera Analyses Ltd.).

The ATR spectra were recorded using a Bruker IFS 48 FTIR instrument with a Specac 25 reflection ATR optics. The spectral resolution of the infrared spectrometer was adjusted to 4 cm^{-1}, and 512 interferograms with an optical range from 4000 to 400 cm^{-1} were accumulated each for background and sample measurement. Post processing of the ATR spectra was performed by using the Bruker Opus software package.

2.6 UV/VIS spectroscopy

UV/VIS diffuse reflection spectra were recorded by a spectrophotometer (Uvikon XL, BIO-TEK Instruments) using an integrating Ulbricht sphere (Labsphere) between 200 and 800 nm at a speed of 200 nm per minute at a bandwidth of 4 nm. Aerosol samples were collected onto Whatman QMA quartz fibre filters. As reference material for the integrating sphere labsphere Spectralon Diffuse Reflectance Standards were used (SRS-99-010). No significant absorption of UV/VIS radiation was observed comparing clean quartz fibre filters to the labsphere standards.

2.7 Temperature programmed pyrolysis mass spectroscopy

This experiment has originally been developed at the Vienna University of Technology in order to analyse the oxidation processes of soot particles from diesel engines (Muckenhuber and Grothe, 2006; Ofner and Grothe, 2007). Soot is a multi-component system, which is extremely difficult to analyse. Therefore, the focus has been set on the controlled fragmentation of the functional groups, which in fact are the key species when discussing reactivity. The same idea has been translated to the analyses of HULIS particles and their related oxidation processes. Aerosol particles were sampled onto quartz fibre filters mentioned above. In TPP-MS experiments the coated

ACPD
10, 17369–17405, 2010

quartz fibre filters were placed in a quartz glass flask, which was evacuated down to 10^{-5} mbar. Then the sample was heated at high vacuum from room temperature up to 900 °C with a heating rate of 10 K min^{-1}. Through a leak valve a small portion of the pyrolysis gases was induced into the UHV of the mass spectrometer (Balzers Prisma 200 QMS). Several mass fragments were recorded as a function of the pyrolysis temperature. To identify decomposing functional groups the mass signals of OH (m/z=17), CO (m/z=28) and CO_2 (m/z=44) were exploited. Peaks were allocated to the decomposing functional groups (Muckenhuber and Grothe, 2006).

2.8 Ultrahigh resolution mass spectroscopy

Ultrahigh resolution mass spectroscopy was performed at the Helmholtz Centrum Munich, Germany with the Bruker 12 Tesla APEX Q Ion Cyclotron Resonance Fourier Transform Mass Spectrometer (Bremen, Germany). Electrospray injection was followed in negative mode with an APOLLO II electrospray source in flow injection at 2 µl/min (Gaspar et al., 2009). The molecular formulae were batch-calculated by a software tool, written in-house and achieving a maximum mass error of ≤0.2 ppm. The generated formulae were validated by setting sensible chemical constraints (N rule, O/C ratio ≤1, H/C ratio ≤2n+2, element counts: C≤80, H unlimited, O≤60) in conjunction with an automated theoretical isotope pattern comparison (Gaspar et al., 2009). Even enabling up to 3 N and 3 S resulted in mainly CHO types of elementary formulae (only few formulae corresponding to impurities were found as CHNO, CHOS and CHNOS).

The filters were pushed by the cap into Eppendorf 2-ml vials, extracted directly with 1 ml of methanol and centrifuged in the same Eppendorf vials to be ready for injection.

ACPD
10, 17369–17405, 2010

3 Experimental

The precursors for the SOA were catechol (Riedel-de Haën, 32101, p.a.) and guaiacol (Sigma Aldrich, G5502). Ozone was produced from pure oxygen (Riessner-Gase, >99.995%) using a silent discharge ozonizer (Sorbios, GSG 0012).

For each precursor three experiments were carried out: 1. formation of SOA in the dark with O_3 only, 2. formation of SOA at simulated sunlight with O_3 only and 3. formation of SOA at simulated sunlight with O_3 and 25% relative humidity. No particle formation could be observed from the reaction of guaiacol with O_3 in the dark – hence no data is presented.

For aerosol size distribution experiments 100 ppb of the precursor and 500 ppb of ozone were used to study the formation of the SOA. FTIR experiments had to be performed at higher concentrations (5 ppm precursor substance and 20 ppm ozone) because of the detection limit of the long-path-FTIR spectrometer.

ATR samples were collected onto the KRS-5 crystal two hours after SOA formation with duration of 30 min at an aerosol flow of 6.5 cm^3 sec^{-1}. About 10^8 aerosol particles were collected each for ATR measurements from medium particle concentrations of 10^5 particles cm^{-3} at a collection efficiency of about 90%.

For UV/VIS spectroscopy, FEG-SEM imaging, TPP-MS and ultrahigh resolution mass spectroscopy aerosol particles formed at higher precursor concentrations (5 ppm) were sampled onto the specified filter materials.

4 Results and discussion

4.1 Formation of SOA – aerosol size distribution and particle imaging

The mass concentrations and size distributions of the formed SOA strongly depend on the environmental conditions in the aerosol smog-chamber, as shown in Figs. 2 and 3. The aerosol mass distributions were derived from volume distributions with an as-

ACPD
10, 17369–17405, 2010

sumed density of 1.4 g cm^{-3}(Coeur-Tourneur et al., 2009). Aerosol formation yields are influenced by the presence of simulated sunlight and relative humidity. The precursors play a decisive role in this formation process. The catechol precursor is found to generate one order of magnitude more aerosol mass than the guaiacol precursor at simulated sunlight conditions. At a relative humidity of 25% these yields are observed to increase significantly. Particle size distributions show similar medium particle diameters for all experiments between 40 and 70 nm. The half-width of the particle size distribution from SOA produced in the dark is lower than that compared to the experiments of simulated sunlight. So UV/VIS radiation has an influence on particle formation, not only concerning the overall aerosol mass, but also on the particle size distribution as shown in Fig. 3. Particle formation seems to be fairly complete after about 30 min. Subsequently, only aggregation of small particles takes place, as demonstrated by the slow change of the aerosol diameters and the FEGSEM image in Fig. 4.

For scanning electron microscopy (Fig. 4) higher precursor concentrations were selected to produce sufficient SOA particle density. Therefore, aerosol particles are slightly larger than the mean value observed in the aerosol size distributions (Figs. 2 and 3). The particles with diameters between 100 and 250 nm are of nearly perfect spherical shape. No structured surface texture is visible. Chain- and cluster-like aggregates of those particles have also been observed.

4.2 Formation of SOA – long-path FTIR spectroscopy

To study the aerosol formation process, especially the change of chemical bonds inside the aerosol particles, long-path FTIR spectra were recorded using the 40 m White cell inside the aerosol smog-chamber. Every 10 min 256 single scans were sampled. According to the composition of the gas phase (N_2, O_2, CO_2 and O_3) and the chemical structure of the precursors, only vibrational modes containing carbon, oxygen, and hydrogen can be expected.

The SOA formation process of particles from catechol or guaiacol as precursors is

ACPD
10, 17369–17405, 2010

finished after less than 30 min (Fig. 5). At the beginning of the SOA formation the spectra of the organic gas or particle phase can be assigned to the catechol molecule (Socrates, 1980). The aromatic ring is represented by the vibrations 1620, 1510 and 1480 cm^{-1} which are typical of the aromatic stretching vibration ν(C=C). The sharp absorption at 3063 cm^{-1} matches the ν(C–H) stretching vibration, the two absorptions at 3671 and 3608 are the respective ν(O–H). Phenolic alcohols have corresponding vibrations at 1364 and 1325 cm^{-1}, where the phenolic ν(C–O) stretching vibration can be found. The absorptions in the range 1272 to 1155 cm^{-1} and the band at 1090 cm^{-1} represent either the aromatic in-plane deformation δ(C–H) or the phenolic deformation mode δ(O–H). The aromatic out-of-plane deformations are the absorptions between 860 and 740 cm^{-1}. The ozone concentration is represented by the absorption at 1043 cm^{-1}.

During the aerosol formation process most of those absorptions are slightly decreased and the formation of some new bands can be studied. Although the sharp maxima of the phenolic ν(O–H) vibration decrease, new ν(O–H) vibrations are formed, indicated by the broad absorption at about 3330 cm^{-1}. At the high-frequency shoulder of those bands the absorption at 3450 cm^{-1} increases as well. This band might be assigned to the intra molecular bonded ν(OH) of –O···H···O=. Atmospheric aerosols are highly oxidized. This can be inspected by the strong carbonyl stretching vibration in the range 1850 to 1680 cm^{-1}. Two main regions can be identified in this band, an absorption at 1792 cm^{-1} indicating the ν(C=O) of esters, anhydrides, carboxylic acids and peroxides and an absorption at 1730 cm^{-1} indicating quinones, ketones and other aromatic and aliphatic ν(C=O) vibrations. More detailed characterization of the carbonyl stretching region was reported recently using an aerosol-flow-reactor coupled to an infrared transmission cell (Ofner et al., 2010). The increasing vibration at 1416 cm^{-1} could be interpreted as the δ(O–H) deformation vibration in combination with the ν(C–O) stretching vibration of carboxylic acids or phenols. Strong hints at aliphatic or aromatic ether formation are given by the vibration at 1118 cm^{-1}. This vibration might represent the aliphatic or aromatic ν(C–O) stretching vibration of ethers.

ACPD
10, 17369–17405, 2010

The presence of carboxylic acids is underlined by the appearance of an absorbance at 955 cm^{-1} indicating the out-of-plane deformation vibration δ(O–H).

The decrease of the sharp maxima, which can be assigned to the aromatic ring vibrations, points at partial ring opening reactions. However, aromatic and unsaturated structures are still present in the resulting aerosol particles. Hence, the resulting organic molecules still contain higher oxidized benzene fragments.

Comparing the infrared transmission spectra of organic aerosols formed at different ambient conditions highlights functional differences not only because of the different precursors but also because of the varied ambient conditions (Fig. 6). The ν(C–H) stretching vibrations of the aromatic hydrogens at 3063 cm^{-1} are stronger degraded at wet conditions. This seems to be strongest with the "wet" guaiacol aerosol because of the weak structure of the aromatic ring caused by the methyl ether group. The absorptions at 3010, 2960 and 2855 cm^{-1} which only appear in the guaiacol aerosol are allocated to the methyl ether group. This group is lost during the aerosol formation process – strongest at wet conditions. Carbonyl containing functional groups implying ν(C=O) between 1850 and 1690 cm^{-1} cannot be characterized in detail. The ν(C=C) stretching vibration of the aromatic ring at 1620 cm^{-1} for the catechol aerosol is shifted down to 1606 cm^{-1} for the guaiacol aerosol because of the enhanced total mass of the precursor molecule. The same shift appears for the aromatic stretching vibration at 1510 cm^{-1} to 1507 cm^{-1}. The degradation of the phenolic group at 1364 and 1325 cm^{-1} is visible for all five ambient conditions, although the band at 1325 cm^{-1} is not visible in the spectra of guaiacol aerosol. The aromatic ring deformation vibrations at 1272 and 1155 cm^{-1} also degrade during the conversion of the precursor. Differences within this frequency range agree to the lowered symmetry of guaiacol. Similar to the formation process of catechol and guaiacol aerosol are the degradation processes of main structural elements and entire functionalities. Main differences can be explained by the additional methyl ether of guaiacol and therefore by the lowered symmetry and increased mass of the precursor. Ambient conditions influence the relative intensities of degradation.

ACPD
10, 17369–17405, 2010

4.3 ATR infrared spectroscopy of aerosol particles

Different formation pathways of SOA from catechol lead to different chemical properties of the formed aerosol (Fig. 7). According to the long-path FTIR spectra the major absorptions can be assigned the same way. The aromatic structure of the SOA is indicated by the –C=C- aromatic stretch vibration at 1620 cm^{-1}. Also a broad absorption in the range of the aromatic C–H stretch vibration (3100–3000 cm^{-1}) verifies this assumption. The aliphatic C–H stretch vibration is less pronounced at 2960 cm^{-1} in the guaiacol aerosol. Also the absorptions at 860 and 740 cm^{-1} of the =C–H out-of-plane deformation vibrations belong to the aromatic system of the organic aerosol.

SOA from catechol formed without solar simulation at 0% relative humidity has the C=O stretch vibration at 1716 cm^{-1}. This band indicates aryl-aldehydes, α,β-unsaturated carboxylic acids, α,β-unsaturated aldehydes and α,β-unsaturated esters. At simulated sunlight conditions this band shifts to 1740 cm^{-1}, where the vibrations of saturated ketones, aldehydes, and esters are located. Absorptions in the range of 3200–2500 cm^{-1} might belong to intramolecular-bonded ortho-phenols and the O–H stretch vibration of carboxylic acids. The broad structured absorption between 1400 and 1000 cm^{-1} implies O–H deformation and C–O stretch vibration combinations of aliphatic and aromatic alcohols. The band at 1196 cm^{-1} might – apart from structural features – also belong to the C–O stretch vibration in Ar–O–Ar or Ar–OH, shown by all SOA samples. Hence, the absorption at 1045 cm^{-1}, which is masked by ozone in the gas phase spectra in the long-path absorption spectra, might belong to the C–O aliphatic stretch vibration of R–O–Ar. Aromatic or α,β-unsaturated esters in the dark-formed SOA might be indicated by the bands at 1716, 1295, 1196 and 1118 cm^{-1}. Carboxylic acids are represented by the ν(C=O) at 1740 cm^{-1}, the ν(C–O) and δ(O–H) at 1416, 1317 and 1295 cm^{-1} and the broad ν(O–H) from 3100 to 2500 cm^{-1}.

ATR-spectra of SOA from guaiacol imply the asymmetric stretch (2960 cm^{-1}) and asymmetric deformation (1440 cm^{-1}) vibrations of the $-CH_3$ group. The intensity of those vibrations are reduced at wet conditions, because the $-CH_3$ group is destroyed

ACPD
10, 17369–17405, 2010

by the reaction with the OH radical. All other vibrations can be explained in the same way as it was done for SOA from catechol.

The combination of these two different FTIR methods allows us to allocate infrared group-frequencies to the functional groups and structural elements listed in Table 1.

4.4 Diffuse reflectance UV/VIS spectroscopy of aerosol particles

The diffuse reflectance UV/VIS spectra of the different aerosol particles from catechol and guaiacol are dominated by a broad absorption up to 600 nm, which is in good agreement with the brown colour of aerosol samples (Fig. 8). The main absorptions of the two precursors catechol and guaiacol in the UV/VIS range are at about 220 and 275 nm, related to the $\pi \rightarrow \pi^*$ transition of the aromatic system and the $n \rightarrow \pi^*$ transition of the lone pairs of the hydroxyl substituents. Within the broad absorption of the organic aerosol particles there occur three main absorptions at 212, 254 and 333 nm, which are represented in all different types of organic aerosol from catechol and guaiacol. One additional absorption at 292 nm is only represented in the catechol dark SOA. This transition seems to be destroyed by UV/Vis radiation.

4.5 Temperature programmed pyrolysis mass spectra of solid aerosol phase

The background corrected TPP mass spectra of the five aerosol types are well structured for the masses 17 (OH), 28 (CO) and 44 (CO_2) (Fig. 9). Peaks below 150 °C are not interpreted because of outgassing of physically adsorbed molecules like H_2O, N_2, CO and CO_2 which might pollute the signals of pyrolysing functional groups. Based on the thermal stability of oxygen containing functional groups and their fragments in soot (Muckenhuber and Grothe, 2006) peak maxima and relative peak intensities can be identified in the SOA in Fig. 9 according to the corresponding temperatures in the different types of aerosol (Table 2).

Very important functional groups in the aerosol particles are carboxylic acids and lactones. Two thermal instabilities of carboxylic acids occur at 270 and 340 °C for both

ACPD
10, 17369–17405, 2010

m/z 17 and 44. There are small differences in the relative intensities of those two acids. The *m/z* 44 signal assigned to lactones is very intense for all aerosol particles except guaiacol SOA light and wet. Further carboxylic anhydrides, phenols and carbonyls and quinones are represented in the TPP mass spectra. Ethers might be represented at 680 °C, but the resulting *m/z* 28 signal is is imperceptible.

The thermal analysis of functional groups is in good agreement with the vibrational spectra, confirming that highly oxidized functional groups play a major role but demonstrating that also lower oxidized groups are present in the aerosol particles. While enhancing the oxidation ability by changing the environmental conditions, carboxylic acids which are stable at higher temperatures (320 °C) increase. However, carboxylic acids at lower temperatures (270 °C), carbonyls and quinones decrease. Minor increases could be observed at carboxylic anhydrides and phenols. The amount of lactones seems to be stable at different simulated environmental situations, except for guaiacol SOA light and wet, where the peak is missing completely.

4.6 Ultrahigh resolved mass spectra of aerosol composition

The methanol extracts from the filter samples exhibit a Gaussian signal distribution between 150 and 900 Da (Fig. 10a) with multiple signals in each nominal mass (Fig. 10b and c) in negative mode electrospray ICR-FT/MS. The polymers showed thousands of signals as exemplified in Fig. 10b and c that are calculated into individual CHO elementary compositions. In the presence of light, the chemical diversity of the samples significantly increased for both catechol- and guaiacol-based mixtures; water however did not have the same impact. The ICR-FT/MS *m/z* signal distribution between the catechol- and guaiacol-aerosol extracts is very similar, and only a detailed description on the elementary composition level shows signals that are typical of the catechol or guaiacol origin.

Hundreds of calculated elementary compositions were transformed into atomic H/C and O/C ratios for a representation on van Krevelen diagrams (Hertkorn et al., 2007, 2008). Based on only one molecular precursor the resulting aerosols cover a major part

ACPD
10, 17369–17405, 2010

of the possible CHO compositional space. Previous ICR-FT/MS analysis on organic aerosols obtained from chamber experiments based on α-pinene ozonolysis enabled the differentiation of various monomers to oligomers (Reinhard et al., 2007); in this case however the mixtures are characteristic with continuous H/C values restricted between 0.5 and 1.5 and O/C values ranging from 0.3 up to 1 with gradual changes in peak intensity with increasing oxygen content. This behaviour is particular to the catalyzed oxidative polymerisation of these phenols to polyphenols as described in the early days of soil humic substance chemistry (Stevenson, 1994). Organic aerosol from catechol and guaiacol is typically characterized by high oxygen to carbon ratios, indicating the presence of ortho-benzenes or 1,6-oxidized conjugated olefins (Fig. 10). Catechol-based mixtures also significantly differ from guaiacol (Fig. 11) with signals of increased intensity having lower oxygen content and higher aromaticity. Based on the chemical structure of the precursors, hydrogen to carbon ratios above 1 and high oxygen contents can only be explained by condensations and the addition of hydroxyl groups to the unsaturated carbon structure, which is confirmed by the broad ν(O–H) absorption in the FTIR spectra.

5 Conclusions

Synthetic SOA from catechol and guaiacol produced in aerosol smog chamber experiments fulfills the physical chemical characteristics of humic like substances according to their analytical properties described above and can be used as atmospheric model substances for HULIS. Environmental conditions like solar radiation or relative humidity influence not only physical properties like aerosol size distributions or formation yields but also chemical properties like the total amount of oxidized sites and amount and types of functional groups. Further, we could show that the accessibility of precursors for atmospheric oxidizers is an important parameter for the HULIS properties. This is demonstrated by the obstructive effect of the methyl ether group of guaiacol.

HULI-SOA from catechol and guaiacol typically exhibits small particles with diame-

ACPD
10, 17369–17405, 2010

ters between 40 and 90 nm, built up by a very fast formation process. Those particles have a nearly perfect spherical morphology, indicating their atmospheric origin.

The chemical transformation from the gaseous precursor to the final aerosol particle is distinguished by the formation of different functional groups and disappearance of well defined structural elements of the entire benzene ring. The aromatic or olefinic structural element, an important attribute for atmospheric HULIS, still persists in the aerosol particle. The variation of simulated sunlight or relative humidity results in different degrading structural elements like aromatic ν(C=C) and ν(C−H) stretching vibrations and different pronounced oxygen containing functional groups like shifting of ν(C=O) vibrations. Especially ATR-FTIR spectra of synthetic HULI-SOA from catechol and guaiacol show many common features with reported natural HULIS according to structural elements and functional groups. Apart from the aromatic and olefinic structure especially functional groups like carboxylic acids, anhydrides and esters fulfil these qualities.

Light absorption of those organic particles ranges up to 600 nm into the visible region of the electromagnetic spectrum. Thus, HULI-SOA samples are light brown coloured. This optical feature indicates absorption processes according to conjugated aromatic or olefinic structures with a high amount of chemically bound oxygen.

The O/C ratio between 0.3 and 1 is in good agreement with the reported O/C ratios for LV-OOA (low-volatile oxidized organic aerosol) and SV-OOA (semi-volatile OOA) (Jimenez et al., 2009). Further, the medium value of 0.6–0.7 fits the described oxidation state of atmospheric HULIS very well (Graber and Rudich, 2006). But the measured medium H/C ratio of 1 is too low for atmospheric HULIS. The reported values are between 1.6 and 1.7. The difference between the H/C values is explained by the absence of aliphatic side chains in the SOA from catechol and guaiacol. Hence, SOA from those precursors represents the aromatic and olefinic oxidized core structure of atmospheric HULIS very well. Still aliphatic parts of atmospheric HULIS are not represented. The medium mass of organic molecules in the particles of 300–450 Da is close to natural HULIS samples.

ACPD
10, 17369–17405, 2010

HULI-SOA from catechol and guaiacol provides several features according to natural HULIS aerosol samples. Especially the high molecular weight caused by the aromatic system and the polycarboxylic acidic functionality matches those properties. Due to the easy preparation it is applicable for lab-scale measurements of organic aerosol processing in aerosol smog chambers or aerosol flow reactors. HULI-SOA could perform like SV- and LV-OOA using aerosol-smog-chamber experiments close to natural conditions. Different stable aged modifications of SOA from catechol and guaiacol could be obtained. The use of different FTIR methods combined with TPP-MS allows us to identify the position of carbon-bonded oxygen at different functional groups (Tables 1 and 2). Therefore the chemical characterization according to functional groups and structural features of the organic aerosol is possible without the need of analyzing every single compound accounting for the particle formation.

Acknowledgements. This work was supported by the Deutsche Forschungsgemeinschaft within the HALOPROC project and by the European Union within the EUROCHAMP project.

References

Andreae, M. O. and Crutzen, P. J.: Atmospheric aerosols: biogeochemical sources and role in atmospheric chemistry, Science, 276, 1052–1058, 1997.

Andreae, M. O.: A new look at aging aerosols, Science, 326, 1493–1494, 2009.

Bröske, R., Kleffmann, J., and Wiesen, P.: Heterogeneous conversion of NO_2 on secondary organic aerosol surfaces: A possible source of nitrous acid (HONO) in the atmosphere?, Atmos. Chem. Phys., 3, 469–474, doi:10.5194/acp-3-469-2003, 2003.

Coeur-Tourneur, C., Tomas, A., Guilloteau, A., Henry, F., Ledoux, F., Visez, N., Riffault, V., Wenger, J. C., and Bedjanian, Y.: Aerosol formation yields from the reaction of catechol with ozone, Atmos. Environ., 43, 2360–2365, 2009.

Coury, C. and Dillner, A. M.: A method to quantify organic functional groups and inorganic compounds in ambient aerosols using attenuated total reflectance FTIR spectroscopy and multivariate chemometric techniques, Atmos. Environ., 42, 5923–5932, 2008.

Cowen, S. and Al-Abadleh, H. A.: DRIFTS studies on the photodegradation of tannic acid as

ACPD

10, 17369–17405, 2010

a model for HULIS in atmospheric aerosols, Phys. Chem. Chem. Phys., 11, 7838–7847, 2009.
Fierz, M., Kaegi, R., and Burtscher, H.: Theoretical and experimental evaluation of a portable electrostatic TEM sampler, Aerosol Sci. Tech., 41, 520–528, 2007.
Fine, P. M., Cass, G. R., and Simoneit, B. R. T.: Chemical characterization of fine particle emissions from the fireplace combustion of woods grown in the Southern United States, Environ. Sci. Technol., 36, 1442–1451, 2002.
Forster, P., Ramaswamy, V., Artaxo, P., Berntsen, T., Betts, R., Fahey, D. W., Haywood, J., Lean, J., Lowe, D. C., Myhre, G., Nganga, J., Prinn, R., Raga, G., Schulz M., and Van Dorland, R.: Changes in atmospheric constituents and in radiative forcing, in: Climate Change 2007: The Physical Science Basis. Contribution of Working Group I to the Fourth Assessment Report of the Intergovernmental Panel on Climate Change, edited by: Solomon, S., Qin, D., Manning, M., Chen, Z., Marquis, M., Averyt, K. B., Tignor, M., and Miller, H. L., Cambridge University Press, Cambridge, UK and New York, 2007.
Gaspar, A., Kunenkov, E., Lock, R., Desor, M., Perminova, I., and Schmitt-Kopplin, P.: Combined utilization of ion mobility- and ultra high resolution-MS to identify multiply charged constituents in natural organic matter, Rapid Commun. Mass Sp., 23, 683–688, 2009.
Graber, E. R. and Rudich, Y.: Atmospheric HULIS: How humic-like are they? A comprehensive and critical review, Atmos. Chem. Phys., 6, 729–753, doi:10.5194/acp-6-729-2006, 2006.
Hays, M. D., Fine, P. M., Geron, C. D., Kleeman, M. J., and Gullett, B. K.: Open burning of agricultural biomass: physical and chemical properties of particle-phase emissions, Atmos. Environ., 39, 6747–6764, 2005.
Hertkorn N., Meringer, M., Gugisch, R., Ruecker, C., Frommberger, M., Perdue, E. M., Witt, M., and Schmitt-Kopplin, P.: High-precision frequency measurements: indispensable tools at the core of molecular-level analysis of complex systems, Anal. Bioanal. Chem., 389, 1311–1327, 2007.
Hertkorn, N., Frommberger, M., Schmitt-Kopplin, P., Witt, M., Koch, B., and Perdue, E. M.: Natural organic matter and the event horizon of mass spectrometry, Anal. Chem., 80, 8908–8919, 2008.
Iinuma, Y., Boge, O., Gnauk, T., and Herrmann, H.: Aerosol-chamber study of the alpha-pinene/O_3 reaction: influence of particle acidity on aerosol yields and products, Atmos. Environ., 38, 761–773, 2004.
Jimenez, J. L., Canagaratna, M. R., Donahue, N. M., Prevot, A. S. H., Zhang, Q., Kroll, J. H.,

ACPD
10, 17369–17405, 2010

DeCarlo, P. F., Allan, J. D., Coe, H., Ng, N. L., Aiken, A. C., Docherty, K. S., Ulbrich, I. M., Grieshop, A. P., Robinson, A. L., Duplissy, J., Smith, J. D., Wilson, K. R., Lanz, V. A., Hueglin, C., Sun, Y. L., Tian, J., Laaksonen, A., Raatikainen, T., Rautiainen, J., Vaattovaara, P., Ehn, M., Kulmala, M., Tomlinson, J. M., Collins, D. R., Cubison, M. J., Dunlea, J., Huffman, J. A., Onasch, T. B., Alfarra, M. R., Williams, P. I., Bower, K., Kondo, Y., Schneider, J., Drewnick, F., Borrmann, S., Weimer, S., Demerjian, K., Salcedo, D., Cottrell, L., Griffin, R., Takami, A., Miyoshi, T., Hatakeyama, S., Shimono, A., Sun, J. Y., Zhang, Y. M., Dzepina, K., Kimmel, J. R., Sueper, D., Jayne, J. T., Herndon, S. C., Trimborn, A. M., Williams, L. R., Wood, E. C., Middlebrook, A. M., Kolb, C. E., Baltensperger, U., and Worsnop, D. R.: Evolution of organic aerosols in the atmosphere, Science, 326, 1525–1529, 2009.

Jonsson, A. M., Hallquist, M., and Saathoff, H.: Volatility of secondary organic aerosols from the ozone initiated oxidation of alpha-pinene and limonene, J. Aerosol Sci., 38, 843–852, 2007.

Jonsson, Å. M., Hallquist, M., and Ljungström, E.: The effect of temperature and water on secondary organic aerosol formation from ozonolysis of limonene, Δ^3-carene and α-pinene, Atmos. Chem. Phys., 8, 6541–6549, doi:10.5194/acp-8-6541-2008, 2008.

Khovratovich, N. N., Novikova, T. M., Khmel'nitskii, A. I., Cherenkevich, S. N., and Loban, V. A.: IR spectra of preparations of ozonized pyrocatechin, J. Appl. Spectrosc., 65, 201–205, 1998.

Kundu, S., Kawamura, K., Andreae, T. W., Hoffer, A., and Andreae, M. O.: Molecular distributions of dicarboxylic acids, ketocarboxylic acids and α-dicarbonyls in biomass burning aerosols: implications for photochemical production and degradation in smoke layers, Atmos. Chem. Phys., 10, 2209–2225, doi:10.5194/acp-10-2209-2010, 2010.

Lary, D. J., Shallcross, D. E., and Toumi, R.: Carbonaceous aerosols and their potential role in atmospheric chemistry, J. Geophys. Res., 104, 15929–15940, 1999.

Limbeck, A., Kraxner, Y., and Puxbaum, H.: Gas to particle distribution of low molecular weight dicarboxylic acids at two different sites in central Europe (Austria), J. Aerosol Sci., 36, 991–1005, 2005.

Mainelis, G., Willeke, K., Adhikari, A., Reponen, T., and Grinshpun, S. A.: Design and collection efficiency of a new electrostatic precipitator for bioaerosol collection, Aerosol Sci. Tech., 36, 1073–1085, 2002.

Muckenhuber, H. and Grothe, H.: The heterogeneous reaction between soot and NO_2 at elevated temperature, Carbon, 44, 546–559, 2006.

ACPD
10, 17369–17405, 2010

Najera, J. J., Percival, C. J., and Horn, A. B.: Infrared spectroscopic studies of the heterogeneous reaction of ozone with dry maleic and fumaric acid aerosol particles, Phys. Chem. Chem. Phys., 11, 9093–9103, 2009.
Nieto-Gligorovski, L., Net, S., Gligorovski, S., Zetzsch, C., Jammoul, A., D'Anna, B., and George, C.: Interactions of ozone with organic surface films in the presence of simulated sunlight: impact on wettability of aerosols, Phys. Chem. Chem. Phys., 10, 2964–2971, 2008.
Nieto-Gligorovski, L., Net, S., Gligorovski, S., Wortham, H., Grothe, H., and Zetzsch, C.: Spectroscopic study of organic coatings on fine particles, exposed to ozone and simulated sunlight, Atmos. Environ., doi:10.1016/j.atmosenv.2009.10.043, in press, 2010.
Ofner, J., Krüger, H.-U., Zetzsch, C., Grothe, H.: Direct deposition of aerosol particles on an ATR crystal for FTIR spectroscopy using an electrostatic precipitator, Aerosol Sci. Tech., 43, 1–5, 2009.
Ofner, J. and Grothe, H.: A mechanistic study of the cooperative effect of NO_2 and O_2 on the soot surfaces, Asian Chem. Lett., 11, 57–61, 2007.
Ofner J., Krüger, H.-U., and Zetzsch, C.: Time resolved infrared spectroscopy of formation and processing of secondary organic aerosols, Z. Phys. Chem., in press, 2010.
Olariu, R. I., Barnes, I., Becker, K. H., and Klotz, B.: Rate coefficients for the gas-phase reaction of OH radicals with selected dihydroxybenzenes and benzoquinones, Int. J. Chem. Kinet., 32, 696–702, 2000.
Reinhardt, A., Emmenegger, C., Gerrits, B., Panse, C., Dommen, J., Baltensperger, U., Zenobi, R., and Kalberer, M.: Ultra-high mass resolution and accurate mass measurements as new tools to characterize oligomers in secondary organic aerosol, Anal. Chem., 79, 4074–4082, 2007.
Sax, M., Zenobi, R., Baltensperger, U., and Kalberer, M.: Time resolved infrared spectroscopic analysis of aerosol formed by photo-oxidation of 1,3,5-trimethylbenzene and alpha-pinene, Aerosol Sci. Tech., 39, 822–830, 2005.
Shapiro, E. L., Szprengiel, J., Sareen, N., Jen, C. N., Giordano, M. R., and McNeill, V. F.: Light-absorbing secondary organic material formed by glyoxal in aqueous aerosol mimics, Atmos. Chem. Phys., 9, 2289–2300, doi:10.5194/acp-9-2289-2009, 2009.
Socrates, G.: Infrared Characteristic Group Frequencies, John Wiley and Sons, Wiley, New York, 1980.
Stevenson, F. J.: Humus Chemistry: Genesis, Composition and Reactions, 2nd ed., Wiley, New York, 1994.

ACPD
10, 17369–17405, 2010

Tomas, A., Olariu, R. I., Barnes, I., and Becker, K. H.: Kinetics of the reaction of O_3 with selected benzenediols, Int. J. Chem. Kinet., 35, 223–230, 2003.

Vesna, O., Sax, M., Kalberer, M., Gaschen, A., and Ammann, M.: Product study of oleic acid ozonolysis as function of humidity, Atmos. Environ., 43, 3662–3669, 2009.

Yu, Y., Ezell, M. J., Zelenyuk, A., Imre, D., Alexander, L., Ortega, J., D'Anna, B., Harmon, C. W., Johnson, S. N., and Finlayson-Pitts, B. J.: Photooxidation of alpha-pinene at high relative humidity in the presence of increasing concentrations of NO_x, Atmos. Environ., 42, 5044–5060, 2008

Zellner R., Behr, P., Seisel, S., Somnitz, H., and Treuel, L.: Chemistry and microphysics of atmospheric aerosol surfaces: Laboratory techniques and applications, Z. Phys. Chem., 223, 359–385, 2009.

ACPD

10, 17369–17405, 2010

Table 1. Main infrared group-frequencies assigned to functional groups and structural features observed in SOA from catechol and guaiacol at different ambient conditions by comparing aerosol-smog-chamber long-path FTIR spectra (LP) with ATR spectra (ATR). (w=weak, m=medium, s=strong).

Allocation [cm^{-1}]	overall structure	catechol SOA			guaiacol SOA	
		dark	light	light and wet	light	light and wet
ν(O–H) intramolec. and –COOH	3450	m	m	m	m	m
ν(O–H)	3330	m	m	m	m	m
ν(C–H) aromatic	3063_{LP} 3090_{ATR}	m	w	m	w	w
ν(C–H) of $-CH_x$	2960				m	w
ν(C=O) aryl and unsaturated	$_{ATR}$	1716				
ν(C=O) olfinic and saturated	$_{ATR}$		1740	1740	1740	1740
ν(C=C) aromatic, olefinic	$_{LP}$	1620	1620	1620	1606	1606
ν(C=C) aromatic ring vibr.	$_{LP}$	1510	1510	1510	1507	1507
δ(C–H) of $-CH_x$	1440_{ATR}				m	w
ν(C–O) and δ(O–H) of –COOH	1416_{LP}	s	s	m	m	m
ν(C–O) of –OH	1364	m	m	m	s	s
ν(C–O) of –COOH, R–COO–R	1317_{ATR} 1295_{ATR}	s	m	m	s	s
ν(C–O) of Ar–O–Ar, Ar–OH or R–COO–R	1196	s	s	m	s	m
ν(C–O) of R–O–Ar	1118	m	w	w	w	w
ν(C–O) of R–O–Ar or R–O–R	1045	m	m	m	m	m
δ(O–H) carboxylic acids	955_{LP}	m	w	w	w	w
δ(C–H) out-of-plane	860, 740	m	w	w	s	s

ACPD
10, 17369–17405, 2010

Table 2. Maxima of observed decomposition temperatures of functional groups in a sample of catechol SOA dark (s=strong, w=weak) and comparison with the other conditions (light, light & wet) and material* (where guaiacol SOA dark does not exist because of a lack of reactivity against ozone), leading to the categories increased (↑), equal (=), decreased (↓) and not observed (–) for the functional groups.

Functional group decomposition in soot [°C]	carboxylic acid 270/320	carboxylic anhydride 460	lactone 620	phenol 680	ether 680	carbonyl and quinone 860
catechol dark	s/w	w	s	w	w	s
catechol light	↓/=	↑	=	=	=	↓
catechol light & wet	↓/↑	=	=	↑	=	↓
guaiacol light	=/↑	↑	=	=	=	–
guaiacol light & wet	↓/↑	=	↓	=	=	↓

* Guaiacol SOA dark does not exist because of a lack of reactivity against ozone.

ACPD
10, 17369–17405, 2010

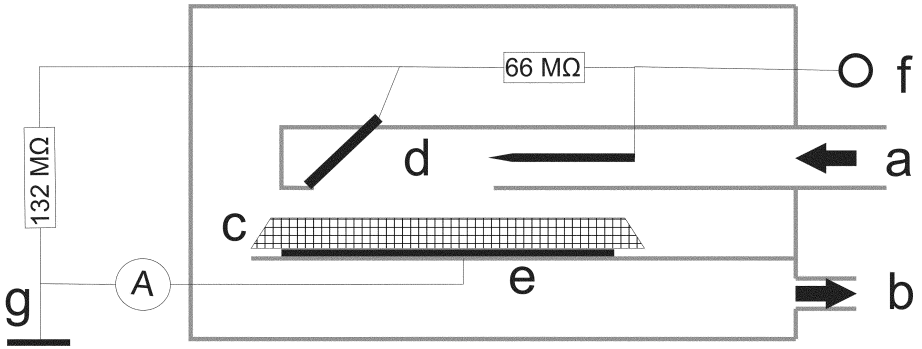

Fig. 1. Two-stage electrostatic precipitator for deposition of aerosol particles onto ATR crystals: a – aerosol inlet; b – vacuum pump (operated at a flow rate between 0.3–3 dm^3 min^{-1}); c – ATR crystal; d – charging and deposition zone; e – copper electrode; f – high voltage supply; g – ground connection; A – electrometer for control of electric current flowing off the ATR crystal.

ACPD
10, 17369–17405, 2010

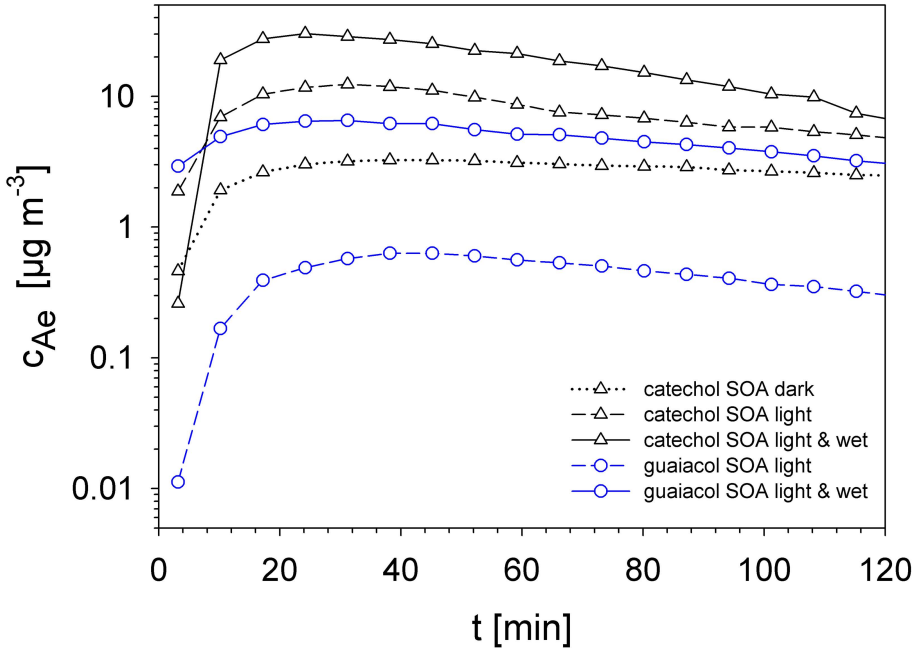

Fig. 2. Evolution of the particle mass concentration over time: the catechol precursor causes higher aerosol mass yields than the guaiacol precursor. Particle formation is strongly influenced by environmental conditions like simulated sunlight and relative humidity.

ACPD
10, 17369–17405, 2010

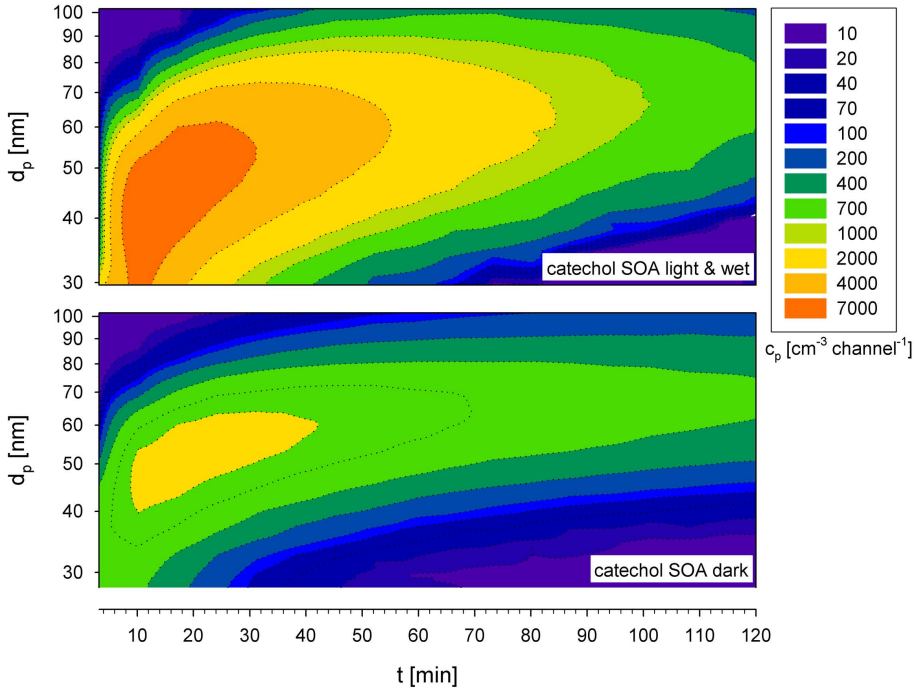

Fig. 3. Change of aerosol size distribution as a function of time: the formed particles reach final mean diameters of 65 nm (dark) and 70 nm (light and wet) after 2 h.

ACPD
10, 17369–17405, 2010

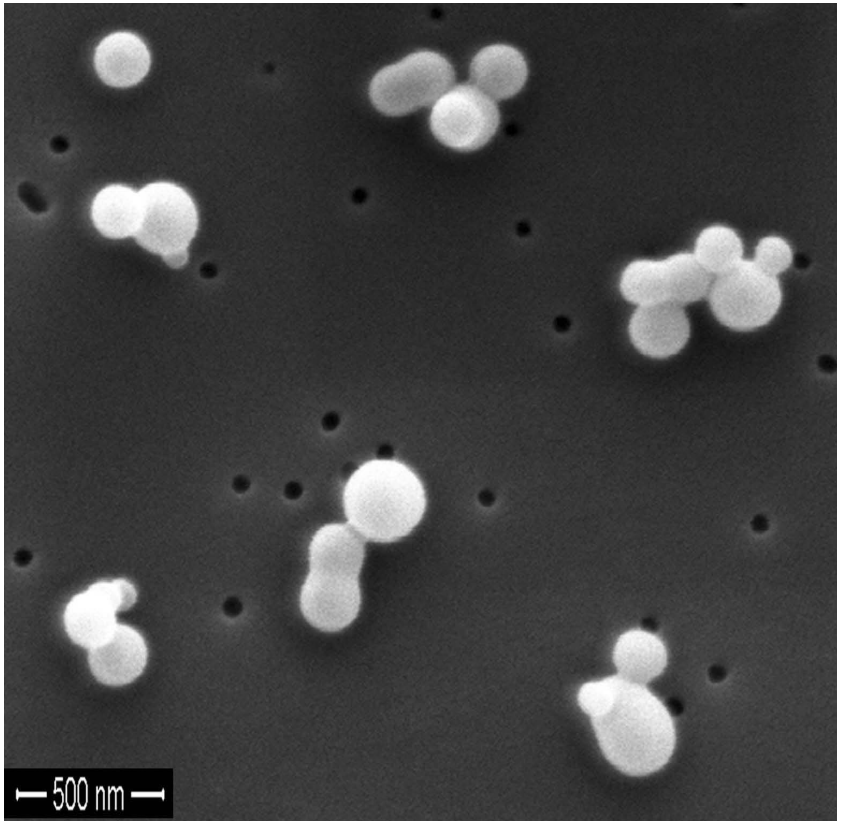

Fig. 4. FEG-SEM image of secondary organic aerosol particles on a polycarbonate filter: nearly perfect spherical particles with no visible surface texture form chain- and cluster-like aggregates. The spherical particles range in diameter from about 80 to 300 nm caused by an increased precursor concentration.

ACPD
10, 17369–17405, 2010

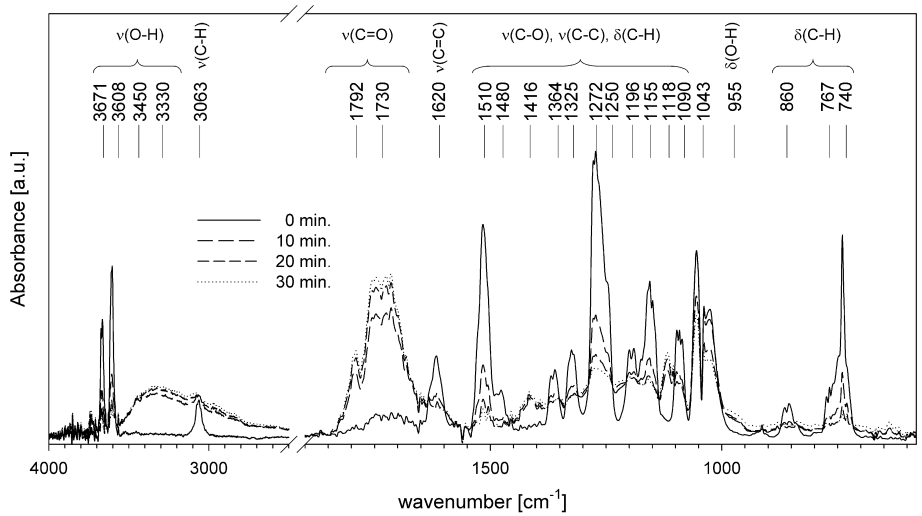

Fig. 5. Time resolved long path FTIR spectra of SOA formation from catechol as precursor: the well defined chemical structure of the precursor migrates to the broad rather undefined structure of macromolecular organic substances.

ACPD
10, 17369–17405, 2010

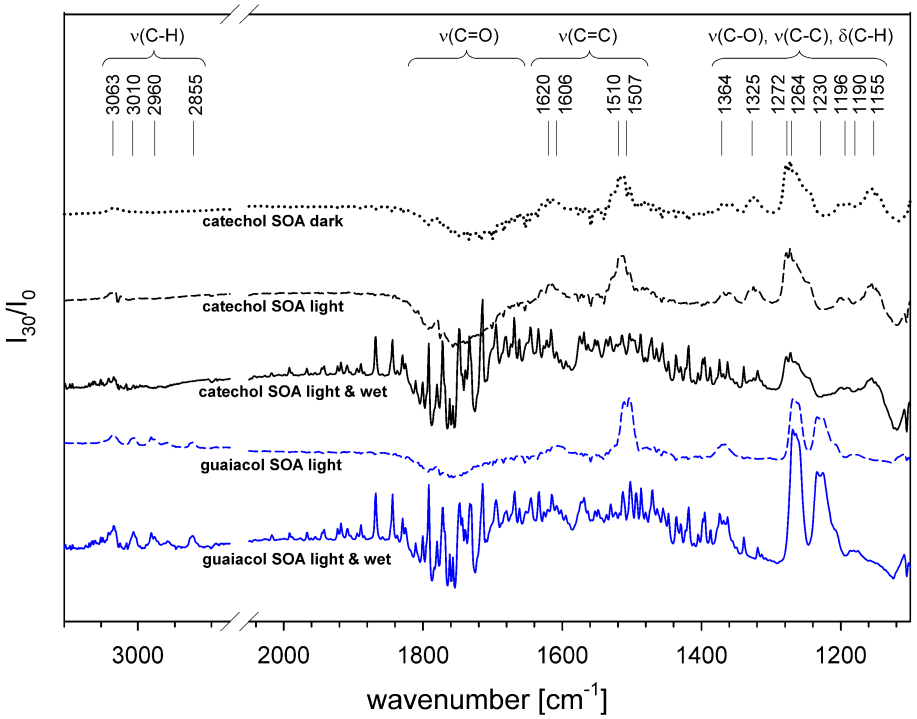

Fig. 6. Transmission difference spectra of the two aerosol precursors compared to the formed SOA at different ambient conditions after 30 min. The spectra are calculated by dividing the single spectra of the different aerosols after 30 min formation by the single spectra at the beginning of aerosol formation.

ACPD
10, 17369–17405, 2010

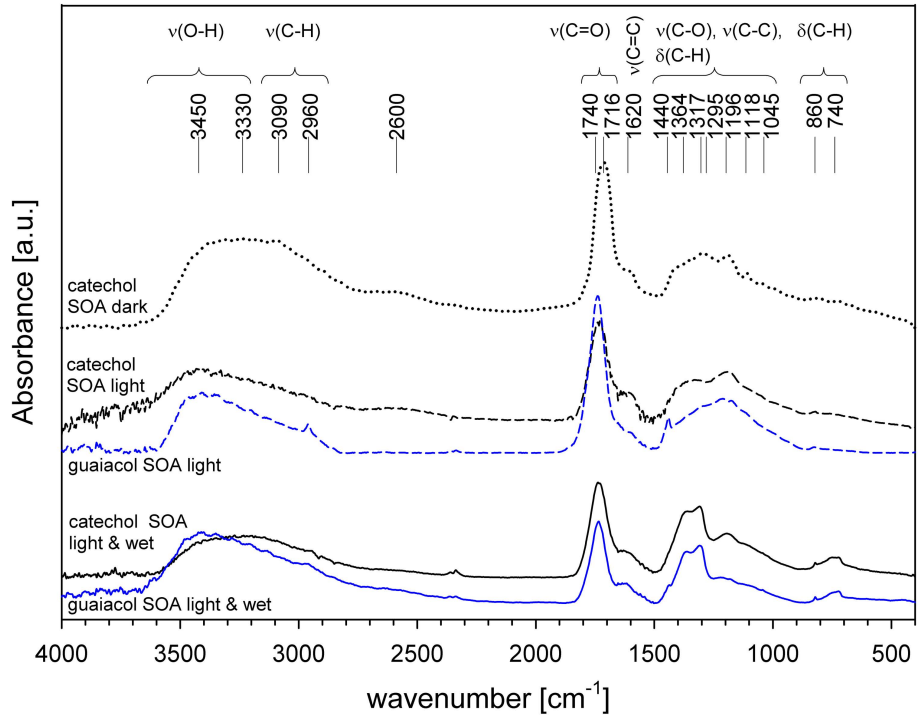

Fig. 7. ATR spectra of secondary organic aerosol particles from catechol and guaiacol sampled by electrostatic precipitation onto the KRS-5 crystal.

ACPD
10, 17369–17405, 2010

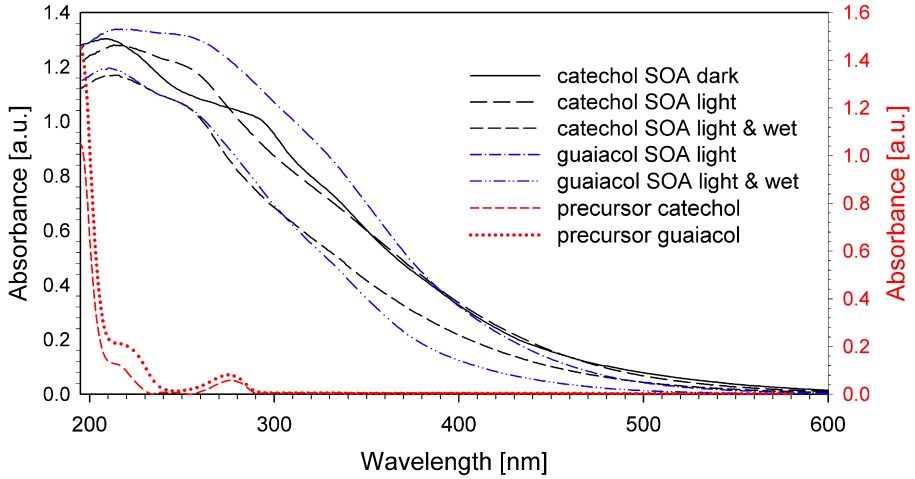

Fig. 8. Diffuse reflectance UV/VIS spectra of SOA from catechol and guaiacol and absorption spectra of the pure compounds.

ACPD
10, 17369–17405, 2010

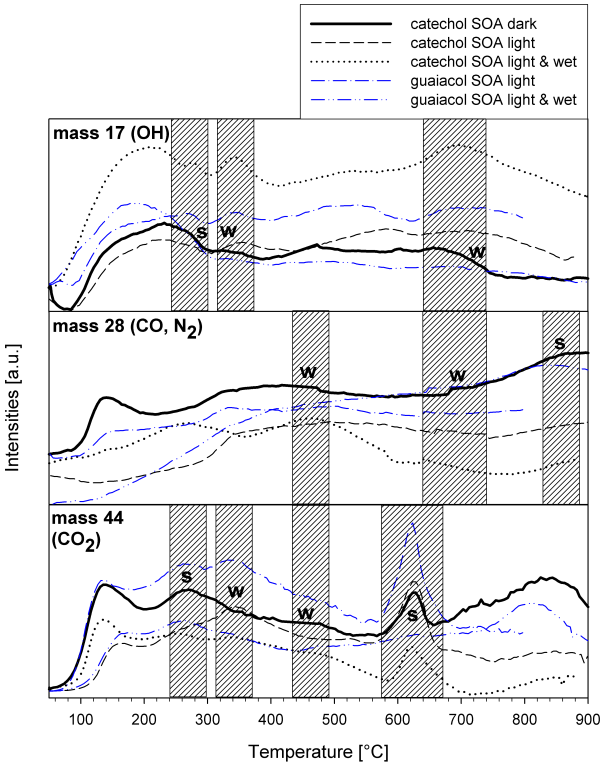

Fig. 9. TPP signals of the three important masses 17 (OH), 28 (CO or N_2) and 44 (CO_2) observed as a function of temperature for the five different SOA particles. The hatched temperature ranges mark observed decomposition of the following functional groups in soot: carboxylic acid (270 and 320), carboxylic acid anhydride (460), lactone (620), phenol (680, *m/z*=17), ether (680; *m/z*=28), and carbonyl and quinone (860). The strengths of these features are indicated as s (strong) and w (weak) for catechol SOA dark, and are compared with each other SOA in Table 2.

ACPD
10, 17369–17405, 2010

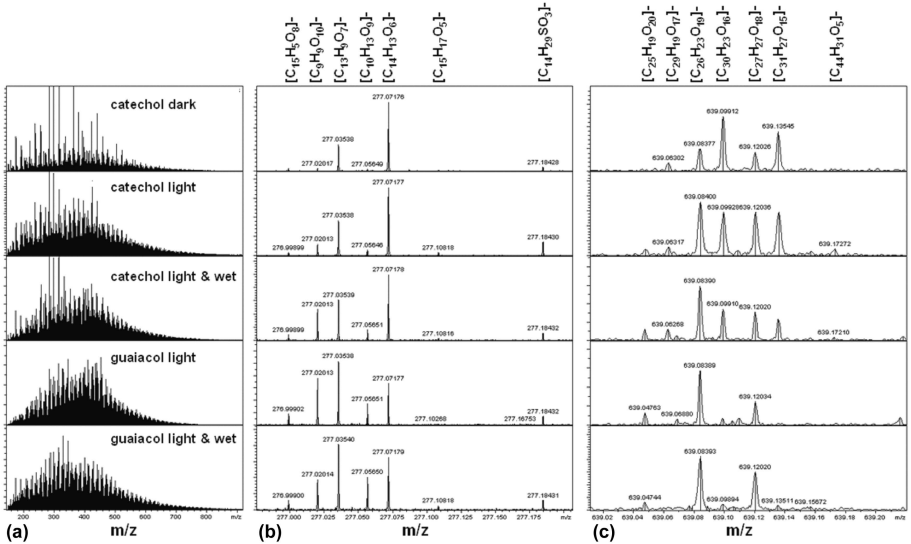

Fig. 10. ICR-FT/MS spectra in the *m/z* range 150 to 900 **(a)** with details on the nominal mass 277 **(b)** and 639 **(c)** showing the assigned elementary composition (error<200 ppb) and the relative signal intensities as a function of precursor, light and wet.

ACPD
10, 17369–17405, 2010

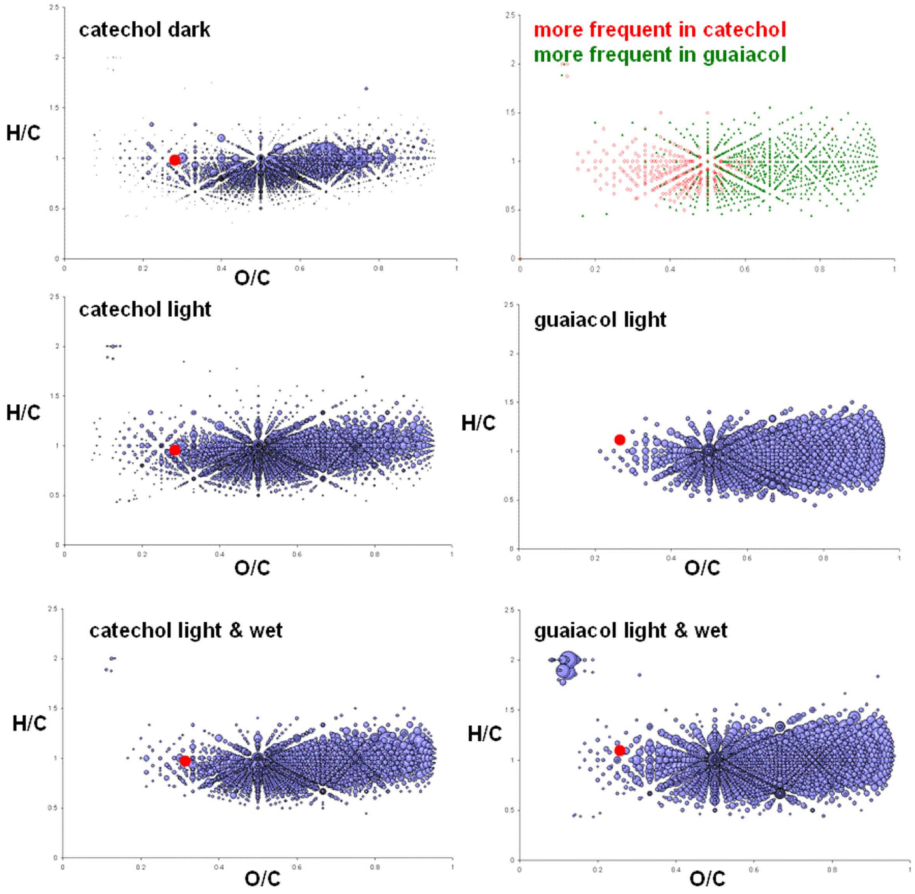

Fig. 11. Van Krevelen diagrams showing the distribution of the H/C and O/C ratios of the ICR-FT/MS data in the CHO compositional space as a function of precursor, light and wet.

ACPD
10, 17369–17405, 2010